JOURNAL OF CHEMICAL INFORMATION AND MODELING

Article

pubs.acs.org/jcim

Effective Screening Strategy Using Ensembled Pharmacophore Models Combined with Cascade Docking: Application to p53-MDM2 Interaction Inhibitors

Xin Xue,[†,‡] Jin-Lian Wei,[†,‡] Li-Li Xu,[†,‡] Mei-Yang Xi,[†,‡] Xiao-Li Xu,[†,‡] Fang Liu,[†,‡] Xiao-Ke Guo,[†,‡] Lei Wang,[†,‡] Xiao-Jin Zhang,[†,‡,∥] Ming-Ye Zhang,[†,‡] Meng-Chen Lu,[†,‡] Hao-Peng Sun,*[,†,‡,§] and Qi-Dong You*[,†,‡]

[†]State Key Laboratory of Natural Medicines, China Pharmaceutical University, Nanjing, Jiangsu 210009, China

[‡]Jiang Su Key Laboratory of Drug Design and Optimization, China Pharmaceutical University, Nanjing, Jiangsu 210009, China

[§]Department of Medicinal Chemistry, School of Pharmacy, China Pharmaceutical University, Nanjing, Jiangsu 210009, China

[∥]Department of Organic Chemistry, School of Science, China Pharmaceutical University, Nanjing, Jiangsu 210009, China

ABSTRACT: Protein−protein interactions (PPIs) play a crucial role in cellular function and form the backbone of almost all biochemical processes. In recent years, protein−protein interaction inhibitors (PPIIs) have represented a treasure trove of potential new drug targets. Unfortunately, there are few successful drugs of PPIIs on the market. Structure-based pharmacophore (SBP) combined with docking has been demonstrated as a useful Virtual Screening (VS) strategy in drug development projects. However, the combination of target complexity and poor binding affinity prediction has thwarted the application of this strategy in the discovery of PPIIs. Here we report an effective VS strategy on p53-MDM2 PPI. First, we built a SBP model based on p53-MDM2 complex cocrystal structures. The model was then simplified by using a Receptor−Ligand complex-based pharmacophore model considering the critical binding features between MDM2 and its small molecular inhibitors. Cascade docking was subsequently applied to improve the hit rate. Based on this strategy, we performed VS on NCI and SPECS databases and successfully discovered 6 novel compounds from 15 hits with the best, compound **1** (**NSC 5359**), K_i = 180 ± 50 nM. These compounds can serve as lead compounds for further optimization.

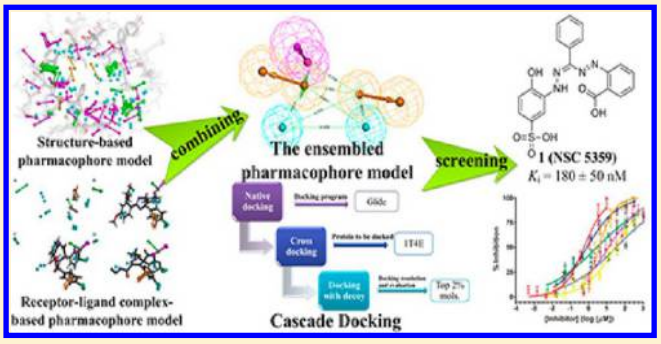

INTRODUCTION

Protein−protein interactions (PPIs) are an emerging class of drug targets essential for biological function.[1] However, there are few protein−protein interactions inhibitors (PPIIs) currently on the market like those inhibitors of G-protein-coupled receptors (GPCR), nuclear receptors, ion channels, and enzymatic targets.[2] Systematic structural analyses of protein−protein interfaces have yielded a highly diverse picture from large and flat to narrow and structured interactions.[3] Targeting PPIs is challenging because it is difficult to mimic these widely spaced weak interactions by using small molecules. Besides, PPIs have performed poorly in high-throughput screenings (HTS) or in other virtual screenings (VS), possibly due to the historical bias of existing chemical libraries.[4] One successful approach for targeting PPIs is to rationally design small molecules mimicking several critical interactions of the hot spots at protein−protein interface.[5] Such a strategy has been successfully applied in the development of several PPIIs[2] (Figure 1) including **BI6** (Xiap/Smac),[6] **Nutlins** (p53/MDM2),[7] **703** (TNFR1A/TNFB),[8] **ABT737** (Bcl/Bak),[9] **CL3** (ZipA/FtsZ),[10] and **RO5963** (p53/MDMX).[11]

Among all the virtual approaches, structure-based pharmacophore (SBP) based and molecular docking based VS are probably the most efficient methods to identify potentially potent compounds from chemical databases containing a large amount of molecules. However, these approaches are thwarted while applied in the discovery of PPIIs for the following problems: (1) SBP models that describe the whole critical features in the PPIs are usually quite large and complicated, thus not suitable for the screening of small molecules; (2) It is a puzzle to select important features that contribute the most to the PPIs, making the simplification of the SBP model very difficult; (3) For molecular docking of a database containing hundreds of thousands of compounds, the computational time available for each compound is very limited, resulting in inaccurate prediction of the binding models, especially for flexible PPIIs. In addition, current scoring functions have much room for improvement in their accuracy of binding affinity prediction.

Received: June 15, 2013
Published: September 19, 2013

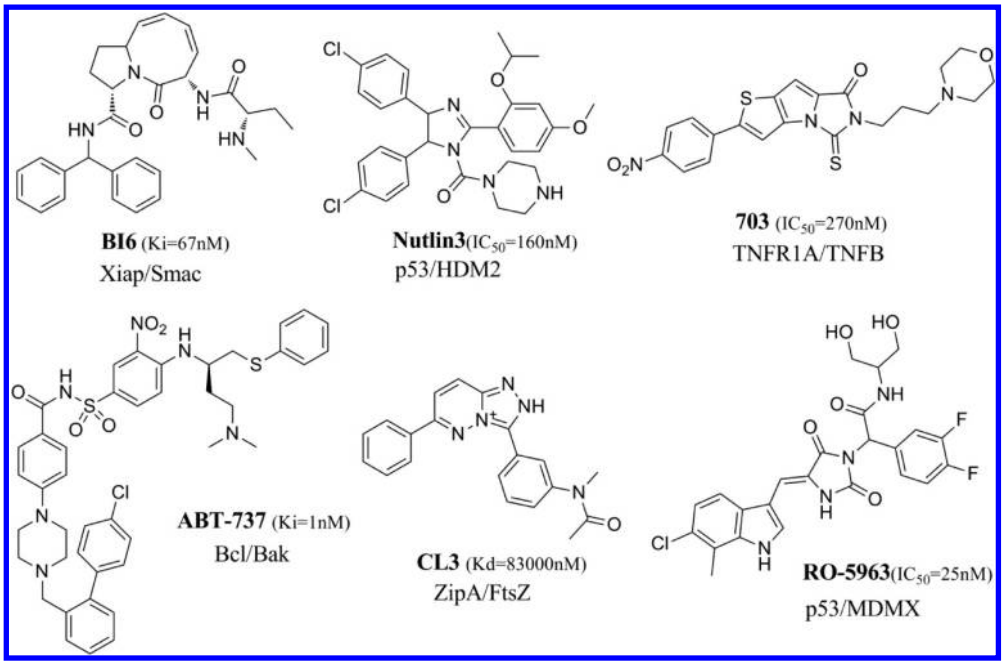

Figure 1. Chemical structures of PPIIs which have been reported.

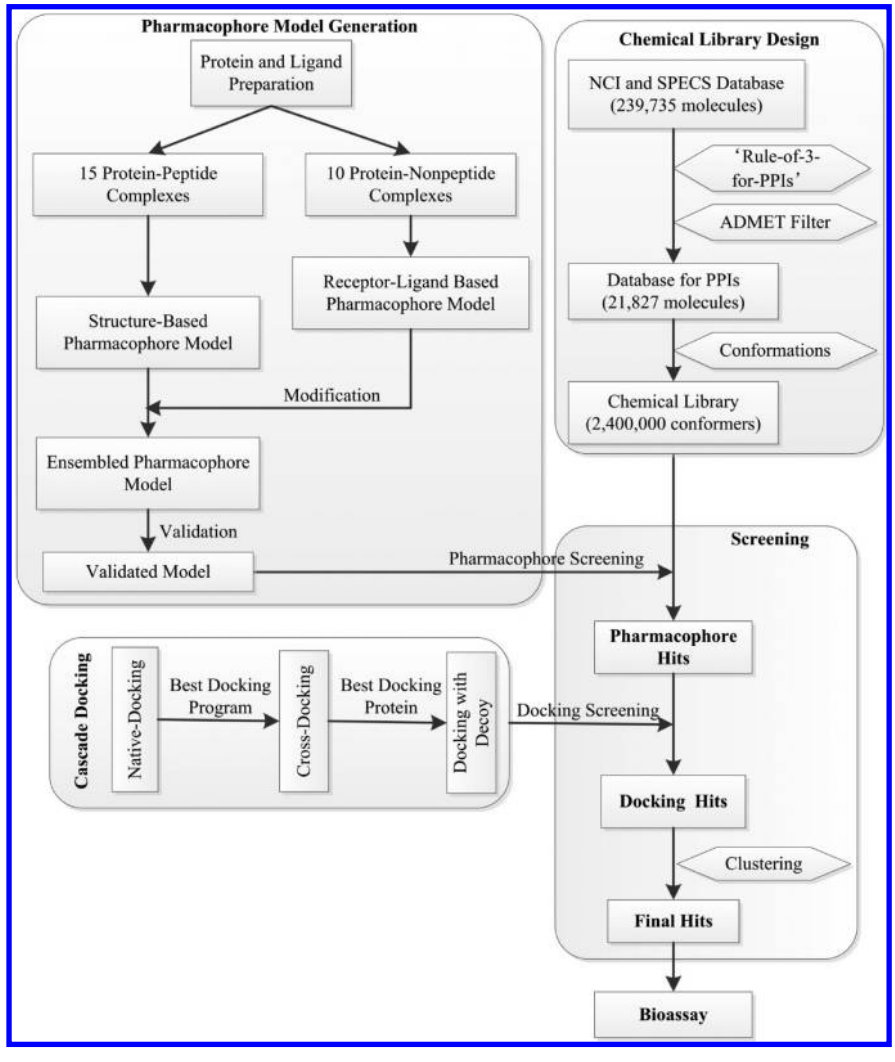

Figure 2. Flow diagram of the pharmacophore generation protocol and cascade docking procedures.

dx.doi.org/10.1021/ci400348f | J. Chem. Inf. Model. 2013, 53, 2715−2729

As a typical PPI, p53-murine double minute 2 (MDM2) interaction plays a pivotal role in regulating the transcriptional activity of tumor cells in human body.[12] p53-MDM2 interaction has long been recognized as a high-risk target due to the fact that proteins generally offered relatively large and flat interacting surfaces which were not readily disturbed by small-molecule drugs. Since the year of 2003[13] various approaches have been developed to identify and design p53-MDM2 interaction inhibitors.[14] These approaches focused on high throughput screening (HTS),[15,16] pharmacophore screening,[17−19] dock screening,[20] *de novo* designing,[21] and mimicking peptides,[22] and several potent small drugable inhibitors were discovered, such as **JNJ26854165**,[23] **RG7112**,[24] **MI-219**,[25] **JNJ-27291199**,[26] and **AM8553**.[27] They possessed good physicochemical properties and showed high binding affinity to MDM2. However, there remains to be an effort for us to enrich the structure types and find novel potent inhibitors. Hence, it is worthy to develop an effective and accurate VS strategy to design novel drugable p53-MDM2 interaction inhibitors.

Herein, we report an effective VS model combining ensembled pharmacophore models and cascade docking for the discovery of novel p53-MDM2 inhibitors (Figure 2). Fifteen SBP models are generated based on a set of cocrystal structures of the p53-MDM2 peptide. The common features among these models are reserved to form a Multiple-Protein-Structures (MPS) based model. However, this model is too large and complicated to be suitable for the alignment of small molecules. For simplification, we used a Receptor−Ligand pharmacophore model (a model focus on Receptor−Ligand complexes based on the LigandScout algorithm[28]) to help select critical features from the MPS model. The ensembled model is then applied for the VS of a PPI database containing over 239,735 compounds derived from National Cancer Institute (NCI) and SPECS databases. The hit compounds are then evaluated for their binding affinities and conformations with MDM2 using a cascade docking method. Fifteen compounds are reserved and evaluated using a quantitative and sensitive fluorescence-polarization based (FP-based) competitive binding assay and *in vitro* antitumor assay using HCT116 $p53^{+/+}$(with wild-type p53) and HCT116 $p53^{-/-}$ (with p53 deleted). Six compounds with novel scaffolds exhibiting potent target-based and cell-based activities can be served as promising lead compounds for further optimization.

MATERIALS AND METHODS

Figure 2 shows the computational protocol that was applied to PPIs. Full details of each step are discussed in the following paragraphs.

Pharmacophore Model Generation. *Protein and Ligand Preparation.* All known MDM2-ligand complex (except PDB code: 1Z1M) structures have been determined by protein crystallography.[19] In the RCSB Protein Data bank (PDB) there were 25 cocrystal structures for the MDM2-ligand (25 cocrystal structures used here were reported before June 2012), all determined by X-ray crystallography, with different resolutions and different ligands, and in some cases with some mutations in the protein sequences. Fifteen MDM2-peptide complex crystals (PDB code: 1T4F, 1YCQ, 1YCR, 2AXI, 2GV2, 3EQS, 3G03, 3IUX, 3JZR, 3JZS, 3LNJ, 3LNZ, 3IWY, 3TPX, 3V3B) were clustered as **Set 1**; 10 MDM2-nonpeptide complex crystals (PDB code: 1T4E, 1TTV, 1RV1, 3JZK, 3TU1, 3LBK, 3LBL, 4ERE, 4ERF, 4DIJ) were clustered as **Set 2** (Table 1). Each

Table 1. Two Sets of MDM2-Ligand Complex Crystals Collected from the PDB Database

Set 1			Set 2		
MDM2-peptide	resolution	sequence	MDM2-nonpeptide	resolution	sequence
1T4F	1.90 Å	23-110	1T4E	2.60 Å	16-111
1YCQ	2.30 Å	21-108	1TTV	NMR	13-119
1YCR	2.60 Å	25-109	1RV1	2.30 Å	25-109
2AXI	1.40 Å	23-114	3JZK	2.03 Å	18-110
2GV2	1.80 Å	25-112	3TU1	1.60 Å	18-110
3EQS	1.65 Å	26-109	3LBK	2.10 Å	26-110
3G03	1.80 Å	25-111	3LBL	1.60 Å	17-110
3IUX	1.65 Å	27-109	4ERE	1.80 Å	17-111
3JZR	2.10 Å	16-112	4ERF	2.00 Å	17-111
3JZS	1.78 Å	26-108	4DIJ	1.90 Å	18-110
3LNJ	2.40 Å	26-108			
3LNZ	1.95 Å	25-109			
3IWY	1.93 Å	26-107			
3TPX	1.80 Å	26-109			
3V3B	2.00 Å	24-110			

structure was prepared using the protein preparation workflow with Prepare Protein protocol in Discovery Studio 3.0 (DS). Missing atoms in residues and missing loop regions were inserted based on SEQRES data. Water and alternate conformations were deleted. Short and medium size loop regions were optimized with the LOOPER[29] algorithm, and the remaining loop regions were minimized in the CHARMm force field. All structures' pK_a were calculated and protonated.[30] The coordinates of 25 MDM2-ligand X-ray crystal structures were transformed into a common reference frame by using 'Multiple Structure Alignment' module in DS.

Structure-Based Pharmacophore Models Generation. SBP models were generated based on 15 complex structures in **set 1** (Table1) with the Ludi[31] algorithm using Interaction Generation protocol in DS3.0. This protocol created a pharmacophore query from a Ludi interaction map which was created in a receptor active site sphere and consists of hydrogen bond acceptor, hydrogen bond donor, and hydrophobic features. These pharmacophore models focused on the 'Lid' domain and 'Gate-Keeper' Tyr100. The generated pharmacophore features of each crystal structure were clustered to ensemble a center feature. Finally 15 pharmacophore queries were generated. Then we aligned the 15 pharmacophore queries and reserved the most common features to generate a structure based pharmacophore model, Hypothesis 1 (Hypo 1).

Receptor−Ligand Based Pharmacophore Model Generation. Ten previously aligned MDM2-nonpeptide complex structures in **set 2** (Table1) were used to construct Receptor−Ligand pharmacophore models. Most of their native ligands, as shown in Figure 3, were recently reported to be evaluated in human clinical trials. The pharmacophore hypotheses were constructed using the LigandScout[28] algorithm by the Receptor−Ligand Pharmacophore Generation module in DS. The LigandScout algorithm allowed the automatic construction of the pharmacophore model from the structural data of the protein−ligand complex. These pharmacophore queries focused on three critical points which were located by Phe19, Trp23, and Leu26 of p53 in the binding pocket. Ten initial queries with their features were aligned and clustered using the Catalyst algorithm to define the center feature. Finally a

dx.doi.org/10.1021/ci400348f | J. Chem. Inf. Model. 2013, 53, 2715−2729

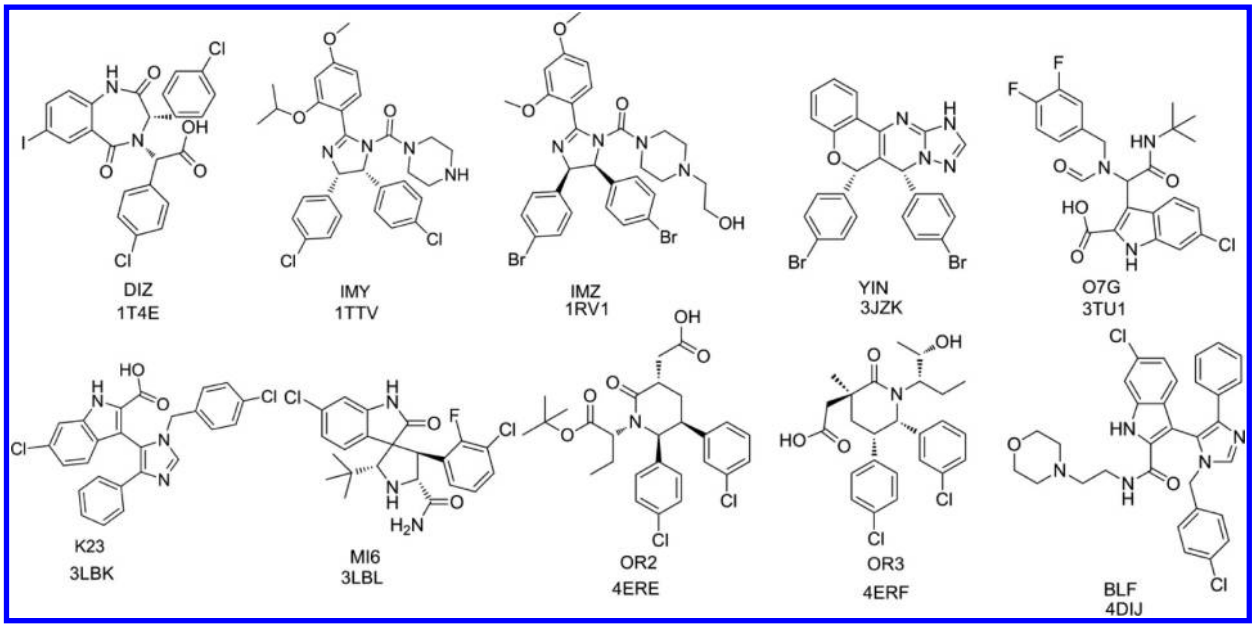

Figure 3. Native ligand structures extracted from 10 MDM2-nonpeptide complexes in **Set 2**.

pharmacophore hypothesis (Hypo 2) based on multiple Receptor−Ligand complex structures were generated.

The Ensembled Pharmacophore Model Generation. How to modify a pharmacophore model based on protein structures is always a perplexing issue. Researchers used a test cluster of active and inactive inhibitors to validate and modify the pharmacophore model. Herein we use a pharmacophore model based on Receptor−Ligand which focuses more attention on ligands. The pharmacophore model built on the Receptor−Ligand complex reflects more features of the interaction between MDM2 and ligands than which built on ligands. The pharmacophore model built on receptor structures can factually represent the energy contributed by critical points in the process of interacting between protein and ligands. However, these hypotheses were usually used to design peptide inhibitors; the features of the model were far away from each other. Besides, there were more pharmacophore features which were not suitable to design small nonpeptide inhibitors. On the other side, the hot spots represented by its pharmacophore features actually approach the flexibility of the protein and the interaction between protein and ligands *in vivo*. Hence, we used pharmacophore models based on the Receptor−Ligand complex to fine adjust the position and size of key features.

Validation of Pharmacophore Models. For validating the reliability of the constructed pharmacophore models, the enrichment factor (EF)[32] was calculated using a decoy database. The EF was calculated using the following formula

$$\mathrm{EF} = \frac{a/n}{A/N}$$

where n = total number of hits, a = the total number of active molecules in the n hits, N = total number of molecules in database, and A = the total number of actives in the database.

The decoy database was built by mixing the 10 ligands (extracted from complexes structures in **Set 2**) (Table 1) with 42 active antagonists (IC_{50} < 1 μM), 91 inactive antagonists (IC_{50} > 100 μM), and 2000 compounds (selected randomly from United States Pharmacopeia). All the compounds were converted to 3D structures, and multiple conformers were generated using the Diverse Conformation Generation module in DS running with the Best conformations option. The energy of each compound was minimized in the MMFF force field.

Chemical Library Design. In view of the structural diversity and availability at the time of study, among the numerous commercial and academic compound databases, the NCI Plated 2007 Database and SPECS Natural Database were selected for the screening purpose. The two databases with 239,735 compounds was filtered by 'Rule-of-3-for-PPIs', which were not similar to well-known Lipinski's 'Rule-of-5', Morelli's 'Rule-of-4',[2] and Congreve's 'rule of three' for fragment-based lead discovery.[33] The 'Rule-of-3-for-PPIs' were 300 ≤ MW ≤ 700 Da, ALogP ≥ 3, number of rings (N_Ring)≥2, number of hydrogen bond acceptors (N_HBA)≥3, number of hydrogen bond donors (N_HBD)≤3. Then the database was calculated the follow Absorption, Distribution, Metabolism, Excretion, and Toxicity (ADMET) properties by Pipeline Pilot (PP) 8.0. The molecules which had unacceptable ADMET properties were removed. Those compounds that passed all of the screening experiments were retained for further study. The filtered database was built of multiconformers by using the 'Build 3D Database' module in DS (best method, maximum number of conformers = 255).

Cascade Docking. *Native-Docking.* The MDM2-nonpeptide complexes (1TTV, 1T4E, 3JZK, 3TU1, 3LBL, 4ERE, 4ERF, 4DIJ) which had the 'Lid' domain were used to conduct Native-Docking. These ligands were docked back into their corresponding protein structures using Gold5.0, Libdock, Flexdock, CDOCKER (DS3.0), and Glide (Schrödinger2009). The docking results were evaluated through comparison of the best docked ligands binding modes with the experimental ones. The root-mean-square deviation (RMSD) was used to compare differences between the atomic distances of the docked poses and the real cocrystallized pose to measure docking reliability. The docking software with the smallest RMSD would be selected to perform Cross-Docking.

Cross-Docking. Eight complexes used in Native-Docking were used to perform Cross-Docking[34] evaluation. The native ligands were docked into all complex structures using the

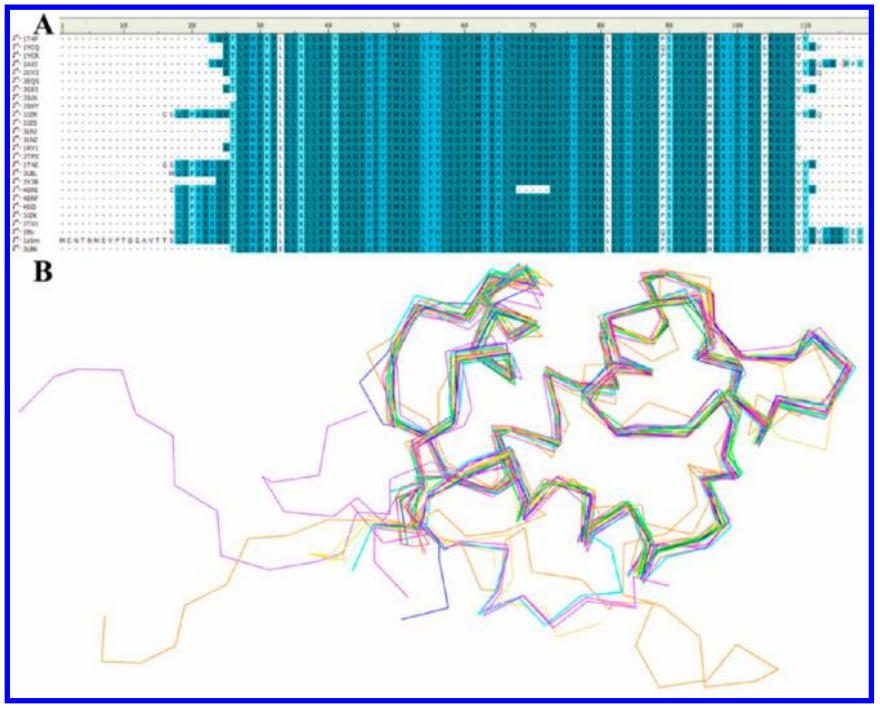

Figure 4. (A) The sequence alignment of 26 proteins. (B) The superimposition of 26 MDM2 structures.

docking software confirmed by Native-Docking. The docking reliability was evaluated by calculating the RMSD difference of each ligand between the reference positions of the ligand in the experimental MDM2-ligand complex and positions predicted by the docking software. Finally the working protein structure was selected which had the smallest RMSD.

Docking with Decoy. To validate the docking results, a decoy database was built. What is more, docking with decoy helps us determine the percentage of the ranked compounds that we should select in the cascade docking. The decoy database was used to validate pharmacophore models previously. The parameters of the docking function were determined by Native-Docking and Cross-Docking. EF in the top 0.5%, 1%, 2%, 3%, 4%, 5%, and 10% of the ranked database was calculated.

Screening. *Pharmacophore Screening.* The chemical database with about 21,827 molecules and approximately 2,400,000 conformers was screened employing the ensemble pharmacophore model using the Search 3D Database module with the fast flexible search method in DS. The index 'Fit value' was calculated to rank the screened molecules. The molecules with the Fit value greater than 3 were retained. Conformers belonged to the same molecule were also ranked, and the best conformer with the highest Fit value remained.

Docking Screening. All the molecules which passed the pharmacophore screening were aligned in Schrödinger2009 and processed the cascade docking with the parameter discussed above. Then compounds were evaluated by consistency scoring functions in Glide and Gold 5.0 using several algorithms: Ludi, Goldscore, Chemscore, ASP, CHEMPLP, LigScore1, LigScore2, Jain, and Ludi Energy Estimate 1. The consistent score was calculated and ranked. 2% of molecules with a ranked consistent score were retained and clustered to 10 sets by their similarity using Tanimoto in DS. Finally, one or two compounds with the highest consistent score were picked out from each set subject to the bioassay.

Bioassay. *In Vitro Antitumor Activity.* The cellular growth inhibitory activity was determined using two human osteosarcoma cell lines, HCT116 $p53^{+/+}$ (with wild-type p53) and HCT116 $p53^{-/-}$ (with p53 deleted, a gift from Dr. Bert Vogelstein, Johns Hopkins University). Cells were cultured in RPMI 1640 medium containing 10% fetal bovine serum (Gemini Bioproducts) at 37 °C in a humidified 5% carbon dioxide humidified incubator. $5-6 \times 10^4$ cells per well were plated in 96-well plates (Costar) for 24 h, and the test compounds (prepared in 100% DMSO as a stock solution) were added in quadruplicate (100 μL per well). Ten different concentrations (from 0 to 100 μM) were tested for each compound. For each assay, the controls included only the medium (blank) and only the cells (positive). After 72 h of incubation, 20 μL of MTT (3-[4,5-dimethylthiazol-2-yl]-2,5-diphenyltetrazoliumbromide) solution (5 mg/mL) was added to each well, and after the samples were shaken for 1 min the plate was incubated further for 4 h at 37 °C. Thiobenzodiazepines were dissolved with 150 μL of DMSO, and the plates were read using Eon (BioTek) at 570 nm. The IC_{50} was then analyzed using GraphPad Prism software.

Fluorescence Polarization Binding Assay. The compounds identified as possible MDM2 inhibitors were purchased from NCI and SPECS database. For testing their binding affinities to MDM2 protein, we performed a sensitive and quantitative FP-based binding assay[17,35−39] using human recombinant His-fused soluble protein MDM2 (residues 1 −118) and a p53-based peptide labeled with a fluorescence tag, termed as PMDM6-F (Anaspec, 10 nM). The K_d value of PMDM6-F with the MDM2 protein was determined to be 3.30 ± 0.12 nM. The fluorescence experiments were performed as described in the literature.[38,39] Briefly, the fluorescence polarization experiments were read on SpectraMax Paradigm Multimode Detection Platform (Molecular Devices) with the 485 nm excitation and 535 nm emission filters. The fluorescence intensities parallel (Intparallel) and perpendicular (Intperpedicular) to the plane of excitation were measured in black 96-well NBS assay plates

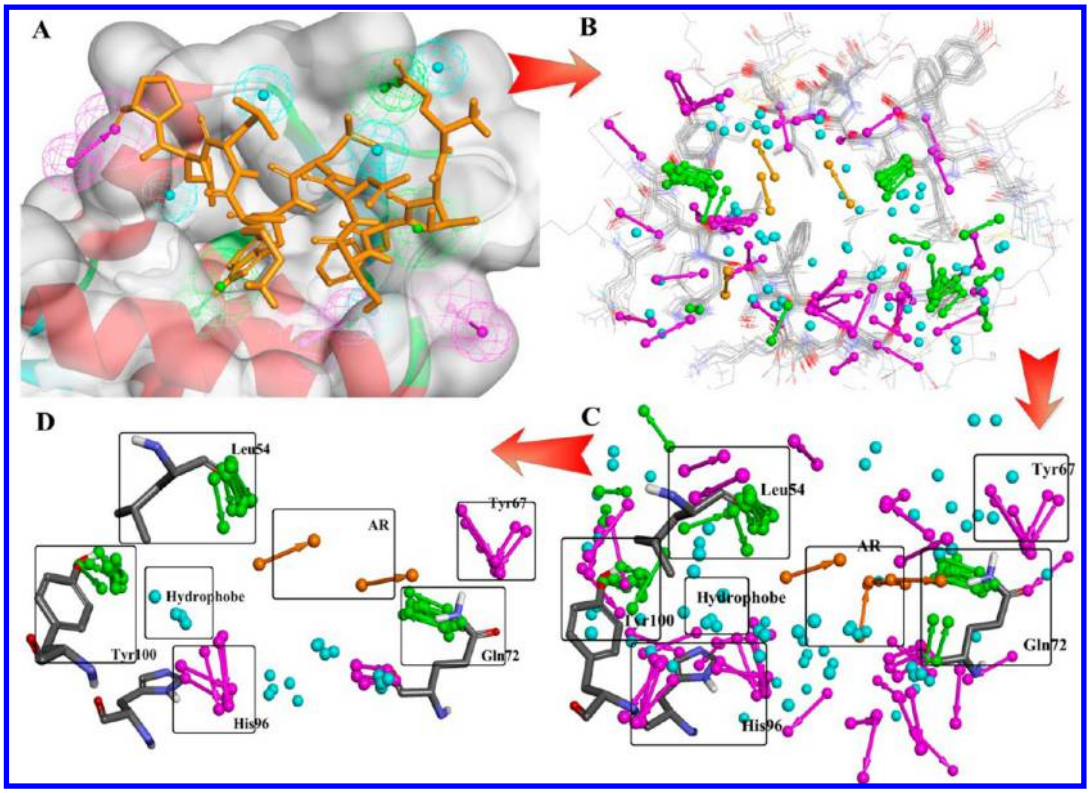

Figure 5. (A) The pharmacophore query was generated by Ludi interaction map based on 1YCQ. Purple is a hydrogen bond donor; green is a hydrogen bond acceptor, and cyan is a hydrophobic or an aromatic element. (B) All 15 pharmacophore queries aligned to define the common features. (C) All common features were clustered to several parts. AR: aromatic ring. Hydrophobe: the hydrophobic core. (D) The key features were retained according to the clustering rule.

(Greiner Microlon) at room temperature. The background fluorescence intensities of blank samples containing the reference buffer were subtracted, and steady-state fluorescence polarization was calculated using the following equation: P = 1000× (Intparallel − GIntperpedicular)/(Intparallel + GIntperpedicular), and the correction factor G (G = 0.998 determined empirically) was introduced to eliminate differences in the transmission of vertically and horizontally polarized light. All fluorescence polarization (FP) values were expressed in millipolarization units (mP). The dose-dependent binding experiments were carried out with serial dilutions (from 0 to 1000 μM) of the tested compounds in DMSO. A 50 μL sample of the tested samples and preincubated MDM2 protein (10 nM) and PMDM6-F peptide (10 nM) in the assay buffer (100 mM potassium phosphate, pH 7.5; 100 μg/mL bovine gamma globulin; 0.02% sodium azide) were added in the black 96-well NBS assay plates (Greiner Microlon) to produce a final volume of 125 μL. For each assay, the controls included the MDM2 protein and PMDM6-F (equivalent to 0% inhibition) and only the PMDM6-F peptide (equivalent to 100% inhibition). The polarization values were measured after 0.5 h of the mixing of all assay components. Binding constant (K_i) and inhibition curves were fitted using GraphPad Prism software and a Web-based computer program developed by Wang.[40]

RESULTS AND DISCUSSION

Proteins and Ligands Preparation Results. Although these 26 protein structures had different lengths, they showed a very high similarity, with 82% identity of the sequence. According to the sequence alignment (Figure 4A), 8 protein−nonpeptide complex structures, 1T4E, 1TTV, 3JZK, 3TU1, 3LBL, 4ERE, 4ERF and 4DIJ, contained the 'Lid' domain (16−24). 4ERE had a section of sequence deletion from 68 to 72. 1Z1M had the longest N-terminal sequence (residues 1−119) which caused the largest RMSD.

Pharmacophore Model Generation Results. Interactions between $MDM2^N$ (N-terminal of MDM2) and $p53^{16-29}$ (residues 16−29 of p53) were essential to generate the SBP model. However, most reported pharmacophore models were mainly built on ligands or rigid receptors. In Galatin's work,[41] a ligand based 3D-QSAR model was developed to predict inhibitory activity. A method of selecting a scaffold candidate for proteomimetic libraries was described as CAVEAT[42] which could be classified as a pharmacophore-based modeling program. This similar scaffold selecting model was also constructed in rigid structures. Then, Yipin Lu and Wang employed an integrated database screening strategy[18] which was a Web-based, flexible pharmacophore searching tool. The pharmacophore did not focus on the flexibility of proteins although it was generated based on proteins structures. In fact, an ideal model should cover both sufficient interaction patterns about $p53^{16-29}$-$MDM2^N$ and common pharmacophore features of flexible receptor structures. Three key points in the binding pocket, Phe19, Trp23, and Leu26 of p53, generated the main scaffold of pharmacophore models which were built on multiple MDM2-ligand crystal structures. Besides, 'Lid' domain was another key point contributing to the p53- MDM2 interaction. As mentioned above, our pharmacophore models focused mainly on those critical interactions of the p53-MDM2 complex. Considering a SBP model's large size which was unreasonable for small compounds, we simplified the SBP model by referring to the Receptor−Ligand complex-based

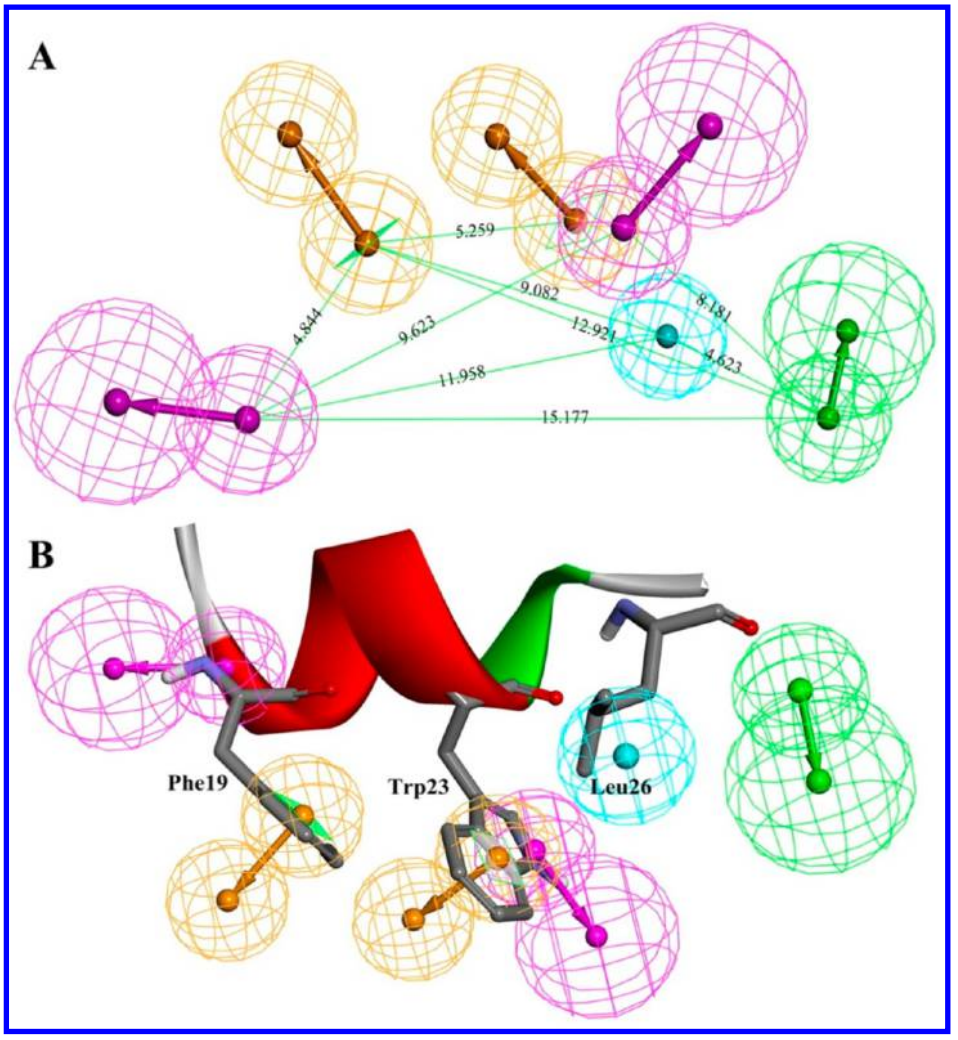

Figure 6. (A) The SBP model consisted of common features. (B) The MDM2 structure-based pharmacophore model with p53 docking in the interacting pocket. Phe19, Trp23, and Leu26 are shown with only backbone atoms. Purple is a hydrogen bond donor; green is a hydrogen bond acceptor, orange is an aromatic ring, and cyan is a hydrophobic feature.

pharmacophore model. Fortunately, the final model had a small size with the longest distance of 6.558 Å between its features. Novel pharmacophore models were generated based on 15 MDM2-peptide crystal structures.

Structure-Based Pharmacophore Model. To construct a SBP model that covers the key points in 15 different queries, the common feature could be generated by a clustering program. Fifteen superimposed MDM2 protein structures with the same coordinate were utilized to generate pharmacophore features via the Ludi interaction map which consisted of a hydrogen bond acceptor (HBA), a hydrogen bond donor (HBD), and hydrophobic features (Figure 5A). Then all 15 pharmacophore queries were aligned to define the common features. As was shown in Figure 5B, there were a few features in the center of the binding pocket, while most were distributed around several subpockets which contained the critical residues like Leu54, Gln72, His96, and Tyr100 of MDM2. Centering on these residues, features were clustered as several sets (Figure 5C). The features around Try67 should be removed because they are located outside the p53 binding pocket. One set that contained less than 4 features and had the distance longer than 1 Å between its features would be deleted. According to the clustering rule, these pharmacophore features could be divided into six sets: three polar feature sets and three nonpolar feature sets (Figure 5D). The central features of each set were finally defined as the common features and constructed the SBP model (Figure 6A). This SBP model (Hypo1) had one hydrogen-bond acceptor (HBA), two hydrogen-bond donors (HBD), two aromatic rings (AR), and one hydrophobic core (HYD). Hydrogen-bond interactions between Leu54, Gln72, and p53 contributed the most to the binding energy of the MDM2-P53 interaction, while Tyr100, known as the 'Gate-Keeper',[43] also had a hydrogen-bond interaction with p53. The hydrophobic core represented the hydrophobic interaction between Leu26 of p53 and MDM2. The last two aromatic rings stood for both $\pi-\pi$ interactions with the MDM2 protein and two anchors of the model. The distance from HBA (Gln72) to HBA (Tyr100) was 15.177 Å which was too long for a nonpeptide molecule, though it matched a small peptide. As was shown in Figure 6B, p53 was mapped on Hypo1 perfectly.

Receptor–Ligand Based Pharmacophore Hypothesis. To acquire more information of MDM2 ligands and to find a way to simplify the SBP model, it was essential to pay more attention to MDM2-nonpeptide complexes. In our work, another pharmacophore hypothesis based on the Receptor–Ligand complex was constructed to modify Hypo1. The hypothesis was generated by the Multi-Protein-Structure (MPS)[17] method which could reflect the protein flexibility.

dx.doi.org/10.1021/ci400348f | J. Chem. Inf. Model. 2013, 53, 2715–2729

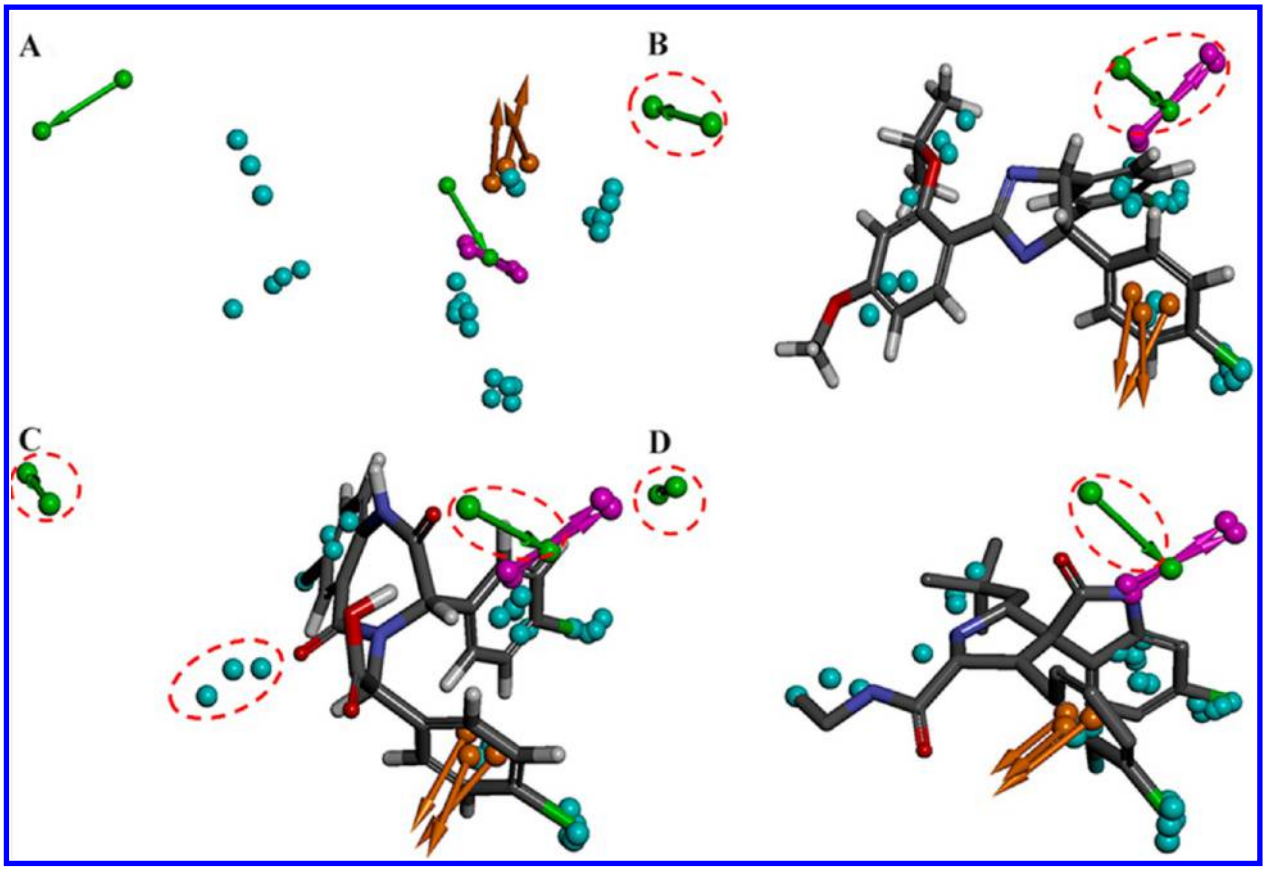

Figure 7. (A)The superimposition of 10 pharmacophore hypotheses; green is HBA; purple is HBD; cyan is AR; and orange is hydrophobic core. The mismatched features are highlighted by red dotted lines in B, C, and D. (B) The superimposition of **Nutlin-3a**. (C) The superimposition of **TDP**. (D) The superimposition of **MI61**.

Among the 10 MDM2-nonpeptide complexes, there were several clinical agents and potential inhibitors, such as **Nutlin-3a**,[44] **MI61**,[39] and **TDP**.[45] All these excellent ligands produced information of molecular shapes and electric charge which could make the pharmacophore hypothesis map out more small MDM2 inhibitors. As mentioned above, features generated from 10 MDM2-nonpeptide complexes were clustered to define the common features (Figure 7A). After that, three clinical inhibitors were docked into the pharmacophore features to delete the unreasonable features. **Nutlin-3a** matched all the hydrophobic cores well except two hydrophilic points (Figure 7B); **TDP** did not match two hydrophilic points and one of hydrophobic core (Figure 7C); **MI61** matched all the features except a distant acceptor core (Figure 7D). The HBA feature located in the upper left of the model was deleted because of its mismatching of any inhibitors. All these features could be clustered to seven sets, and each set generated one common feature with the rule which was used above. The final hypothesis (Hypo2) based on MDM2-ligand complexes had seven features: five HYDs, one AR, and one HBD (Figure 8). The longest distance between these features of Hypo2 was 10.244 Å which was shorter than Hypo1 (15.177 Å). Obviously, Hypo2 had a smaller size than Hypo1 and that was appropriate for nonpeptide inhibitors like **Nutlin-3a** (Figure 7B).

The Ensembled Pharmacophore Model. Hypo2 (the Receptor−Ligand complex-based pharmacophore model) could map out more novel small compounds with diverse scaffolds although it ignored the target flexibility which was essential for a small PPII. Hypo1 (the SBP model) could illustrate the protein flexibility. However, Hypo1 contained too many redundant features to make its size (number of features and the distance between two ends) larger, which caused the inefficiency of pharmacophore-based screening.[46] Therefore, it was necessary to ensemble these two pharmacophore models.

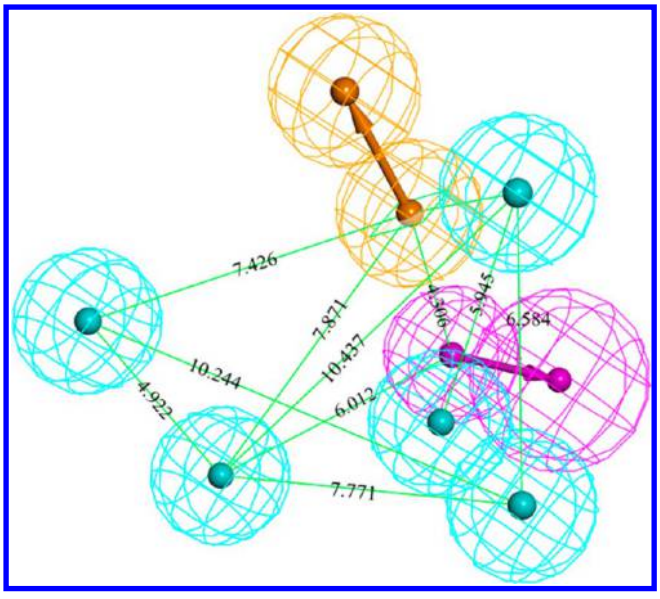

Figure 8. The pharmacophore model built on a Receptor−Ligand complex. Purple is a hydrogen bond donor; green is a hydrogen bond acceptor; and orange is aromatic center.

dx.doi.org/10.1021/ci400348f | J. Chem. Inf. Model. 2013, 53, 2715−2729

Herein we used Hypo2 (containing information of MDM2-nonpeptide complexes) to simplify Hypo1 (focusing on receptor structures) and removed its redundant features. The two pharmacophore models were aligned (Figure 9). It clearly

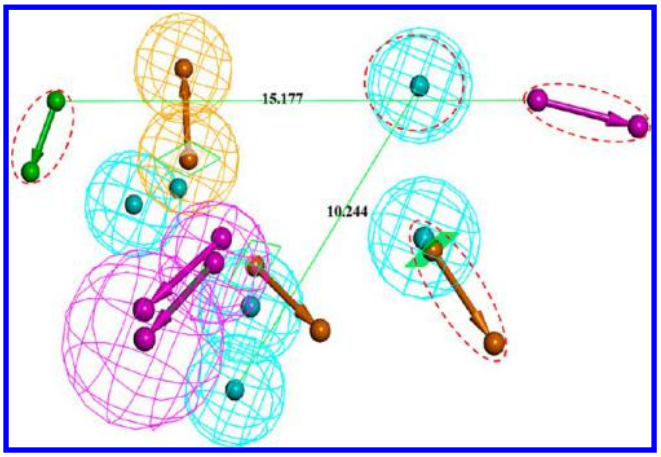

Figure 9. Two pharmacophore hypotheses were aligned to delete the nonessential features (highlighted by red dotted lines). Pharmacophore features with spheres were built on Receptor−Ligand complexes; pharmacophore features with no spheres belonged to the SBP model.

showed that two polar pharmacophore features located at the periphery of the model which had the longest distance (15.177 Å) between each other should be deleted because they were obviously not suitable for screening small molecules. The nearby features were combined together, while the independent ones were deleted. Finally, an ensembled pharmacophore hypothesis (Hypo3) which was more rational for nonpeptide MDM2 inhibitors was generated (Figure 10).

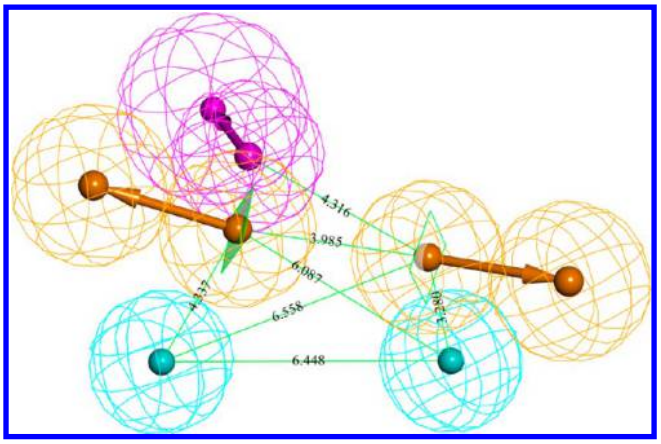

Figure 10. The ensembled pharmacophore model constructed from a structure-based pharmacophore model simplified by a Receptor−Ligand complex-based model.

The basic pharmacophore model had five features: two ARs, two HYDs, and one HBD (Figure 10, Table 2). The longest distance between the features of Hypo3 was 6.558 Å which was nearer than that between Hypo1 and Hypo2. According to the binding mode analysis, three key amino acids (Phe19, Trp23, and Leu26 of p53) were highly emphasized between MDM2 and p53. These interactions between MDM2 and the three critical amino acids of p53 also played important roles in

Table 2. Coordinate of the Ensembled Pharmacophore Model

comprehensive Pharmacophore Generation			
name	X	Y	Z
HBD	45.51	8.29	30.47
AR_Trp23	48.10	10.20	31.11
AR_Phe19	42.78	13.61	33.50
HYD_1	41.93	14.38	30.11
HYD_2	47.16	12.08	27.12

MDM2 nonpeptide ligands. The two ARs deeply inserted the binding pockets which were occupied by two residues, Trp23 and Leu26 of p53. Close to the rings were two hydrophobic features which represented two chlorine atoms modified in the aromatic rings of Trp23 and Leu26. Those four features together composed the main scaffold and shape of Hypo3. Around them were several residues of MDM2: Gly16, Ser17, His96, Try100, Leu57, Ile61, Phe86, and Phe91. The subpocket where HYD_1 occupied consisted of residues Gly16, Leu54, His96, Ile99, and Try100. The subpocket occupied by HYD_2 was much deeper and larger than HYD_1. This subpocket contained aliphatic and aromatic residues: Ile99, Val53, Leu57, Ile61, Leu82, Val93, Ile103 and Phe86, Phe91. The hydrophobic site in the HYD_2 subpocket offered critical van der Waals force between agents and MDM2, which contributed the most energy to the p53-MDM2 interaction. The HBD close to AR_Trp23 and HYD_2 represented the hydrogen-bond interaction between p53 Trp23 indole and the backbone carbonyl of MDM2 Leu54. When the agent approached the binding pocket, this hydrogen-bond interaction guided the agent to the correct position.[47,48] Then these HYDs and two ARs made it stable in the pocket through hydrophobic forces, and the dihedral angles between these four features ensured the scaffold of the agent maintained an optimal tension. Finally, the hydrogen-bond interaction forced the 'Lid' to keep closed.

The Identified Ensemble Pharmacophore Hypothesis Was the Best One. The enrichment of decoy ligands among top ranked compounds was an important criterion for measuring the credibility of a pharmacophore-based screening. The higher the percentage of decoy ligands among the top ranked compounds, the larger the enrichment factor (EF), and the better the performance of pharmacophore-based screening. 42 active and 91 inactive MDM2 inhibitors with inhibitory activity from 10^2 nM to 10^7 nM from the Binding Database and 2000 compounds (selected randomly from United States Pharmacopeia) formed the decoy database.

The predictability of three hypotheses was tested using the decoy database with the same parameters. As was shown in Table 3, Hypo3 had the largest EF with a value of 12.63, while Hypo1 had the least EF value of 1.10. The reason was probably that Hypo1 contained information of key residue structures in the binding domain. These key residues around three p53 subpockets, Phe19, Trp23, and Leu26, were Leu54, Tyr67, Gln72, His96, and Tyr100.[46] When all those features crowded into one pharmacophore model, it enlarged the size of Hypo1 (Figure 6A), which led to reduce the probability for screening hit compounds. Gln72 and Tyr100 features which represented two hydrogen bonds interactions contributed the longest distance (15.177 Å) to Hypo1. Without them, Hypo2 had a smaller size and a greater EF value than Hypo1, although Hypo2 had the most features in all three hypotheses (Figure 8). Because of its concentrated structure, more hits and active

dx.doi.org/10.1021/ci400348f | J. Chem. Inf. Model. 2013, 53, 2715−2729

Table 3. Validation Results for Three Constructed Pharmacophore Models

parameter	Hypo1	Hypo2	Hypo3
number of features in hypothesis	6	7	5
total molecules in database (N)	2143		
total number of actives in database (A)	52		
total hits (n)	34	70	75
active hits (a)	2	11	23
% yield of actives [(a/n) * 100]	5.88	14.29	30.67
% ratio of actives [(a/A) * 100]	3.92	21.57	45.10
false negatives (A-a)	50	41	29
false positives (n-a)	32	59	52
enrichment factor (EF) [$(a/n)/(A/N)$]	1.10	6.05	12.63

compounds were screened out by Hypo2 than Hypo1. Compared to Hypo2, Hypo3 hit twice active compounds, though they had similar total hits (70 for Hypo2 and 75 for Hypo3). Therefore, Hypo3 had less false positives and an increased EF value. These phenomena above could be explained by reviewing the three pharmacophore hypotheses. Hypo3 had 5 features that distributed primarily in Phe19 and Trp23 subpockets which inserted deeply into the p53 binding pocket. These two subpockets had a distance between 3.8 Å and 5.3 Å and contributed the primary hydrophobic and $\pi-\pi$ interactions to the complex like two anchors. Hypo2 had a more or less appropriate size for a small compound like **Nutlin-3a**, but it had too many hydrophobic features (five HYDs and one AR) including useless information in this model. Two HYDs and two ARs of Hypo3 located at the best position (or known as the angles between them) and the skeleton they formed was suitable for designing small nonpeptide inhibitors. While Hypo1 contained information of protein structures and Hypo2 contained information of ligands, Hypo3 combined Hypo1 and Hypo2. Hence, the appropriate size and key pharmacophore features in proper angles made Hypo3 the best pharmacophore model.

Chemical Library Design. Until recently, it had been standard practice to filter drug candidates with Lipinski's 'Rule-of-5' criteria[49] to enhance the drugability of the hits from VS. A statistical analysis[2] (Xavier Morelli et al.) of the 39 PPIIs defined the generic profile of a PPI inhibitor compound that could be further developed to a more druggable inhibitor. Xavier Morelli developed 'Rule-of-4' criteria[2] to describe PPIIs. In our work, chemical properties of the native ligands extracted from 10 MDM2-nonpepride complex structures were preferentially calculated. The properties, shown as Table 4, were not similar with Lipinski's 'Rule-of-5' or Xavier Morelli's 'Rule-of-4'.

Table 4. Generic Profile of the Native Ligands Belonged to the MDM2-Nonpeptide Complex

PDB code	native ligand	MW	ALogP	N_Rings	N_HBA	N_HBD
1T4E	DIZ	581	4.876	3	4	2
1TTV	IMY	567	6.363	3	4	1
1RV1	IMZ	686	5.764	3	6	1
3JZK	YIN	536	6.067	4	4	1
3TU1	O7G	477	2.61	3	4	2
3LBK	K23	461	5.332	5	3	1
3LBL	MI6	449	4.029	2	3	3
4ERE	OR2	519	5.871	2	5	1
4ERF	OR3	477	5.38	2	4	2
4DIJ	BLF	573	6.211	5	4	2

N_Rings of most compounds was more than 3 (average value 3.2, thus N_Rings $\geq$ 3). The number of hydrogen bond acceptors was more than 3. In conclusion, our criteria used here could be defined as 'Rule-of-3-for-PPIs': 300 $\leq$ MW $\leq$ 700, ALogP $\geq$ 3, N_Rings $\geq$3, N_HBA $\geq$ 3, N_HBD $\leq$ 3. These chemical 'Rules-of-3-for-PPIs' properties could be used to filter virtual databases and accelerate the process of hit identification by lowering both cost and time. With the 'Rule-of-3-for-PPIs' criteria 82,026 compounds had passed out from the chemical database containing 239,735 molecules.

ADMET (absorption, distribution, metabolism, excretion, and toxicity) profiles played critical roles in the discovery/development of drugs.[50] It was estimated that 40−60% of new chemical entity failures was due to poor ADMET properties.[51] Hence, during virtual screening ADMET descriptors allowed researchers not only to eliminate compounds with unfavorable characteristics early to avoid expensive reformulation later but also to evaluate proposed structural refinements that were designed to improve ADMET properties, prior to resource expenditure on synthesis. Herein we used the QSAR models to estimate a wide range of ADMET related properties of small molecules in NCI and SPECS databases in DS3.0. Six descriptors (aqueous solubility, blood brain barrier (BBB) penetration, cytochrome P450 2D6 inhibition, hepatotoxicity, human intestinal absorption, and plasma protein binding) were selected to calculate for estimation. Compounds with good absorption level (level 0 according to DS), optimal solubility (level 3 or 4), low BBB penetrability (level 3), CYP450 2D6 noninhibition, and nonhepatotoxic properties were selected as druggable compounds. Finally, 21,827 molecules were selected from 82026 molecules filtered with 'Rule-of-3-for-PPIs' criteria.

Cascade Docking Results. According to the results of Native-Docking of 8 MDM2 proteins to their native ligands (Table 5), docking using the Glide program (Schrödinger2009)

Table 5. RMSD of MDM2-Ligand Complexes Used for Native-Docking

	Docking Software				
PDB (complex)	Gold5.0	Libdock	Flexdock	CDOCKER	Glide
1T4E	3.3	4.4	4.1	4.6	3.0
1TTV	3.5	4.3	4.1	4.4	3.1
3JZK	3.1	4.7	4.3	4.3	3.1
3TU1	4.0	4.6	4.5	5.0	3.5
3LBL	3.2	4.1	4.3	4.8	3.1
4ERE	3.3	4.8	4.2	4.5	3.2
4ERF	3.6	4.8	4.2	4.2	3.2
4DIJ	3.7	5.1	4.6	4.7	3.3
av[a]	3.5	4.6	4.3	4.6	3.2
std[b]	0.30	0.32	0.18	0.27	0.16

[a]Average RMSD values of native ligand poses referring to their native poses. [b]Standard deviation of these RMSD values.

had the smallest average RMSD and standard deviation (std). Although docking using Flexdock had an approximate std (0.18), its average RMSD was not acceptable. The reproducibility of the Glide program was higher than Gold5.0, Libdock, Flexdock, and CDOOKER programs. Therefore, we used the Glide program to dock proteins with inhibitors. Referring to the result of Cross-Docking (Table 6), docking using 1T4E with various ligands had the smallest average RMSD (3.1) and std (0.12). The difference between 1T4E and the other 7 proteins was obvious. For this reason, Glide and 1T4E were selected to

Table 6. RMSD of Ligands in Cross-Docking Using the Glide Program

	native ligands extracted from complexes									
protein	DIZ	IMY	YIN	O7G	MI6	OR2	OR3	BLF	av[a]	std[b]
1T4E	3.0	3.1	3.2	3.3	3.0	3.1	3.1	3.3	3.1	0.12
1TTV	3.2	3.4	3.3	3.7	2.9	3.5	3.5	3.4	3.4	0.24
3JZK	3.2	3.3	3.1	3.4	3.4	3.5	3.5	3.6	3.4	0.17
3TU1	3.9	3.5	3.4	3.5	3.9	3.5	3.5	3.6	3.6	0.19
3LBL	3.1	3.2	3.6	3.5	3.1	3.4	3.5	3.4	3.4	0.19
4ERE	3.2	3.4	3.5	4.1	3.4	3.2	3.3	3.5	3.5	0.29
4ERF	3.2	3.3	3.5	4.1	3.5	3.2	3.2	3.7	3.5	0.32
4DIJ	3.7	3.4	3.6	4.1	4.0	3.6	3.6	3.3	3.7	0.27

[a]Average RMSD values of native ligand poses referring to their native poses. [b]Standard deviation of these RMSD values.

perform docking screening. However, it was not sufficient enough to verify the docking only through 8 native ligands; the other factors in the docking process should be considered as well.

After that, docking with decoy was used to select hits and evaluate the docking result. By calculating the EF value in different percent of top molecules ranked with score, we could know which percent of ranked molecules hit the most active compounds and reduce the false positive. The results was that the EF value in 0.5%, 1%, 2%, 3%, 4%, 5%, and 10% top ranked molecules were 2.3, 8.1, 10.6, 6.7, 5.4, 1.8, and 0.9. Active compounds increased along with the total selected molecules. When the percent was greater than 2%, the EF value dropped. Hence, the best percent of ranked molecules to be selected was 2%.

Finally, 1T4E was used as the working protein and Glide was used as the docking program and 2% of ranked molecules would remain (Figure 11). With cascade docking, 436

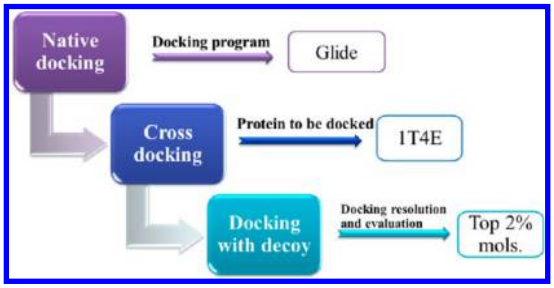

Figure 11. The results of cascade docking used here. Glide was defined as the working docking program, 1T4E was defined as the working protein, and the top 2% were defined as the percent at which ranked molecules were retained.

molecules were chosen and clustered to 10 sets. One or two molecules with the highest consistent score in each set were selected to subject to the bioassay.

Screening and Biological Test results. After screening with ensemble pharmacophore model and cascade docking, fifteen novel compounds with various scaffolds were selected for biological tests. Based on *in vitro* cell proliferation and FP binding assay, six compounds (Table 7) revealed potential inhibitory activity to p53-MDM2 interaction (Figure 12). Among the six active compounds, **1**(**NSC 5359**) had the highest binding affinity with a K_i value of 0.18 ± 0.05 μM. To compare this to other known potent inhibitors of the p53-MDM2 interaction, **Nutlin-3a** had a K_i value of 0.12 ± 0.03 μM in the same competitive binding assay, while two nanomolar inhibitors, **3** (**AF-399/11099019**) and **6** (**NSC 49789**), had K_i

Table 7. Binding Constants (K_i) of 6 Compounds and IC_{50} Values of *in Vitro* Antitumor Activity

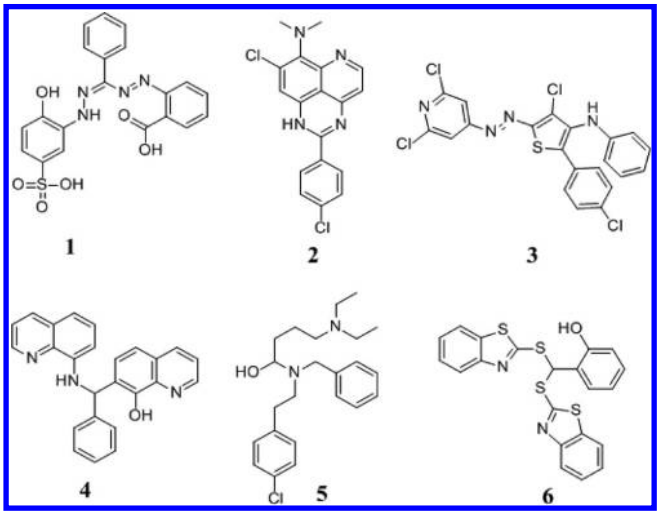

		MTT[b] IC_{50}[c] (μM)		
	K_i[a] (μM)	HCT116($p53^{+/+}$)	HCT116($p53^{-/-}$)	selectivity[d]
1	0.18	85.34	440.07	5.16
2	7.21	22.82	32.82	1.44
3	0.63	69.92	122.11	1.75
4	2.61	8.78	11.18	1.27
5	6.10	27.09	29.92	1.14
6	0.79	64.28	432.12	6.72
Nutlin-3a	0.12	20.22.	24.34	1.20

[a]Values were determined by fluorescence polarization assay. [b]Values are means of three experiments. [c]IC_{50}, compound concentration required to inhibit tumor cell proliferation by 50%. [d]Selectivity was calculated by IC_{50} of HCT116 ($p53^{-/-}$) divided by HCT116 ($p53^{+/+}$).

values of 0.63 ± 0.27 μM and 0.79 ± 0.19 μM. Hence, **1** was 1.5 times less potent than **Nutlin-3a**, but it was 3.52 and 4.39 times more potent than **3** and **6**. The other three compounds, **2** (**NSC 2455**), **4** (**NSC 84096**), and **5** (**NSC 39815**), had micromolar binding affinity to MDM2. It was important to note that none of the hit molecules have been optimized yet, and there existed a possibility for improving the binding affinity of each compound after carefully molecular optimization. Therefore, the discovery of the six new scaffolds with relatively good potency was highly encouraging. The possibility of identification of further novel scaffolds from screening other databases against this VS method should not be dismissed.

To gain more detailed insight into the binding modes of the six compounds, they were docked into the MDM2 protein

dx.doi.org/10.1021/ci400348f | J. Chem. Inf. Model. 2013, 53, 2715−2729

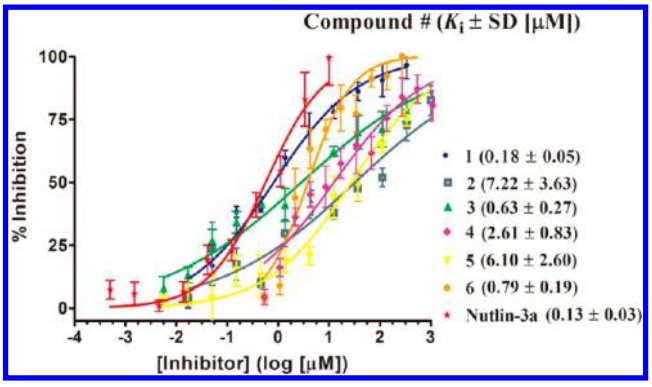

Figure 12. Competitive binding curves of small-molecule inhibitors to MDM2 as determined using a fluorescence-polarization-based binding assay.

(PDB code: 1T4E) with the aligned ensembled pharmacophore model (Figure 13). It was encouraging that compound **1** showed the best binding affinity with MDM2. As was shown in Figure 13A, **1** fully occupied the Phe19 and Trp23 subpockets and matched the pharmacophore model well. Moreover, **1** had two $\pi-\pi$ interactions with Gly16 and Phe19 and one hydrogen bond with Gln59 (Figure 14A). These three interactions were different from classical interactions for p53 and MDM2. It must be noted that Gly16 belonged to the "Lid" domain,[52] hence there was a possibility that **1** interacted with the "Lid" domain and made the ligand-protein complex stable. Similar to compound **1**, **3** had three $\pi-\pi$ interactions with MDM2 (Figure 14B). Due to its aromatic ring stretching out into the solvent, **6** was repulsed by the solvent, which led to an increase in Gibbs free energy. So **6** had a weaker inhibitory activity than **1** and **3** although it matched the pharmacophore model better than **1**. Compound **2** was not mapped well to Hypo3 because of its rigidity. It only occupied the Trp23 subpocket. In our docking test (*S*)-isomer of **4** (K_i = 2.61 ± 0.83 μM) nicely mimicked the three key p53 residues although it had an unreasonable collision with MDM2. Compound **5** showed a weaker binding activity (K_i = 6.10 ± 2.60 μM) to MDM2 than **Nutlin-3a**. Although **5** had a similar position to **Nutlin-3a**, the linker of its two benzene rings was four atoms with sp^3 hybridization which made the distance longer than **Nutlin-3a**. To insert into the p53 pocket, **5** must twist the backbone more which led to the increase of internal energy.

Comparing to their good binding affinities, these compounds had weak cellular growth inhibitory activities. This was probably because of their unreasonable physicochemical properties, bad membrane permeability, or unstable metabolism. The sulfonic group in **1** and sulfur atoms in **6** may lead to the unreasonable physical chemistry properties and bad membrane permeability. The *NN*′ double bonds in compounds **1** and **3** were unstable during the metabolism. It was essential for us to further optimize these compounds and improve physical chemical properties and metabolic stability. Fortunately, they showed excellent cellular selectivity. Antitumor activities in p53 wild-typed cell lines were higher than that in p53 deleted cell lines, which demonstrated the compounds were positive MDM2 inhibitors. The results of cellular growth

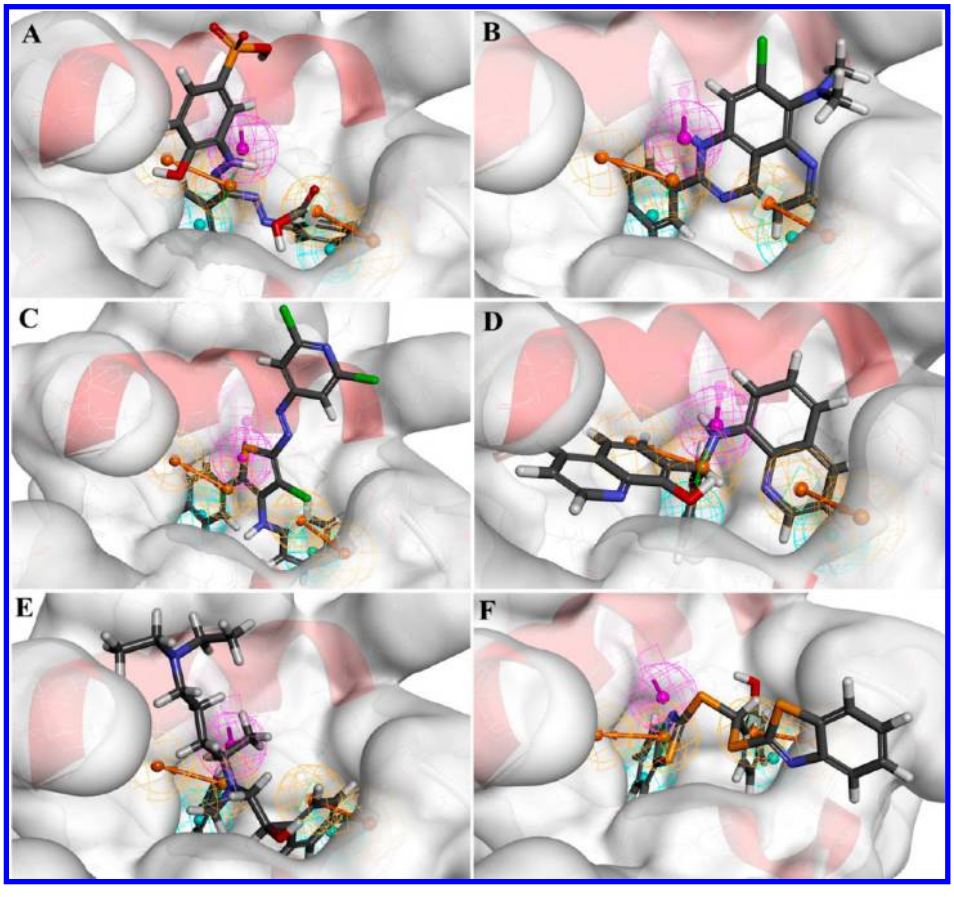

Figure 13. Predicted binding modes of (A) **1**, (B) **2**, (C) **3**, (D) **4**, (E) **5**, and (F) **6** to MDM2. The protein displayed as an α helix with a gray surface. All compounds are shown with only backbone atoms.

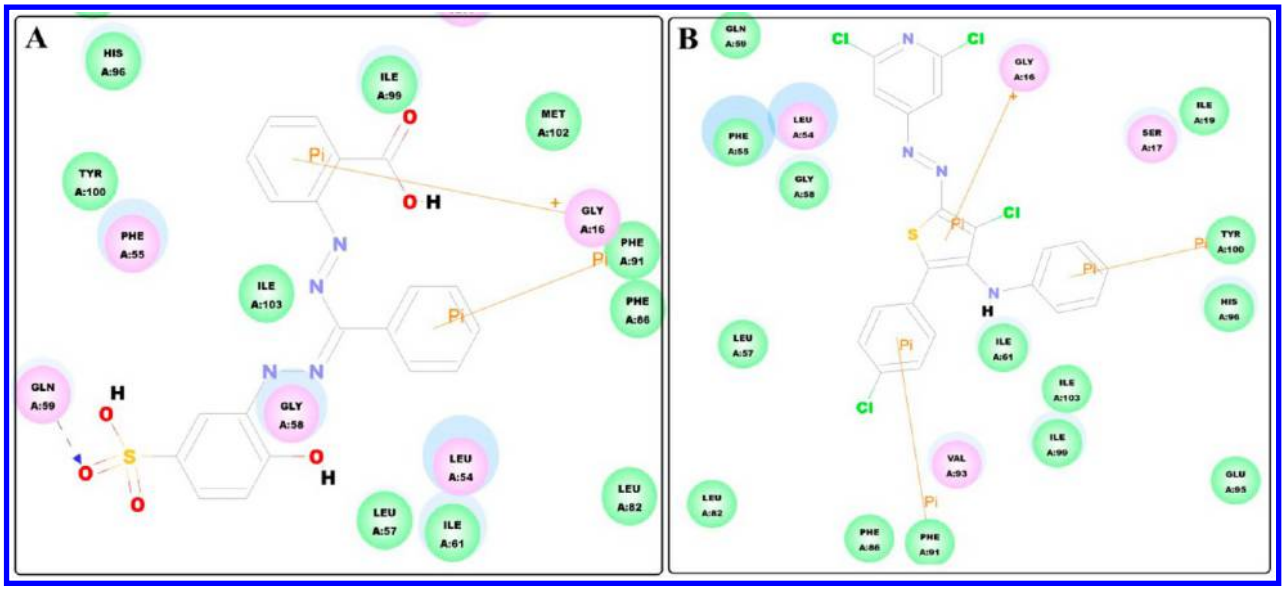

Figure 14. 2D diagram of predicted binding modes of (A) **1** and (B) **3**.

inhibitory activities were consistent with the binding activities. All these above proved that our ensemble pharmacophore model was proper for screening p53-MDM2 interaction inhibitors.

CONCLUSIONS

Successful approaches should optimize each procedure in VS to distinguish actives from false positives. From chemical database to pharmacophore model, docking screening, and result validation, our work has made much effort to optimize the VS strategy special for PPIs. Comparing to classic VS strategy for p53-MDM2 interaction, our VS strategy combined an ensembled pharmacophore model with cascade docking. The chemical database with appropriate chemical space was built for screening drug-like PPIIs. Cascade docking was used to ensure that the protein, the docking program, the resolution, and evaluation were optimal for this docking process with MDM2. We constructed a pharmacophore model, which ensembled a Receptor−Ligand complex-based pharmacophore model to simply the SBP model, with the proper size and shape for screening nonpeptide inhibitors. With the effective VS strategy, six novel scaffolds for inhibiting the p53-MDM2 interaction were identified from a modest database of commercially available compounds. In addition to the success with chemical diversity, the hit rate was nearly 40%. This demonstrated the ability of our VS strategy to broadly and effectively search and identify more diverse inhibitors.

Three potent inhibitors with nanomolar inhibitory activities were identified, **1**, **3**, and **6**, possessing K_i values of 180 nM, 630 nM, and 790 nM respectively. All six novel compounds exhibited good inhibitory activity to MDM2 although some had problems in drugability and metabolic stability. It is the point where lead compounds will be further optimized. In conclusion, our work enriched the chemical diversity of p53-MDM2 PPIIs, and the compounds screened by our VS strategy were demonstrated as potent leads. It is our hope that further development of our VS strategy will introduce a promising new anticancer lead.

AUTHOR INFORMATION

Corresponding Authors

*Phone/Fax: +86 025 83271216. E-mail: sunhaopeng@163.com. Corresponding author address: China Pharmaceutical University, Nanjing 210009, China.

*Phone/Fax: +86 025 83271351. E-mail: youqidong@gmail.com. Corresponding author address: China Pharmaceutical University, Nanjing 210009, China.

Notes

The authors declare no competing financial interest.

ACKNOWLEDGMENTS

This work was supported by the project 81230078 (key program), 81202463 (youth foundation), and 91129732 of the National Natural Science Foundation of China, Program of State Key Laboratory of Natural Medicines, China Pharmaceutical University (No. JKGQ201103), 2012AA020301 of 863 program, 2013ZX09402-102-001-005 and 2010ZX09401-401 of the National Major Science and Technology Project of China (Innovation and Development of New Drugs).

REFERENCES

(1) Wells, J. A.; McClendon, C. L. Reaching for high-hanging fruit in drug discovery at protein-protein interfaces. *Nature* **2007**, *450* (7172), 1001−9.

(2) Morelli, X.; Bourgeas, R.; Roche, P. Chemical and structural lessons from recent successes in protein-protein interaction inhibition (2P2I). *Curr. Opin. Chem. Biol.* **2011**, *15* (4), 475−81.

(3) Gileadi, O.; Knapp, S.; Lee, W.; Marsden, B.; Müller, S.; Niesen, F.; Kavanagh, K.; Ball, L.; Delft, F.; Doyle, D.; Oppermann, U. T.; Sundström, M. The scientific impact of the Structural Genomics Consortium: a protein family and ligand-centered approach to medically-relevant human proteins. *J. Struct. Funct. Genomics* **2007**, *8* (2−3), 107−19.

(4) Sperandio, O.; Reynes, C. H.; Camproux, A. C.; Villoutreix, B. O. Rationalizing the chemical space of protein-protein interaction inhibitors. *Drug Discovery Today* **2010**, *15* (5−6), 220−9.

(5) Popowicz, G. M.; Dömling, A.; Holak, T. A. The structure-based design of Mdm2/Mdmx−p53 inhibitors gets serious. *Angew. Chem., Int. Ed.* **2011**, *50* (12), 2680−2688.

(6) Wu, G.; Chai, J.; Suber, T. L.; Wu, J. W.; Du, C.; Wang, X.; Shi, Y. Structural basis of IAP recognition by Smac/DIABLO. *Nature* **2000**, *408* (6815), 1008−12.
(7) Kussie, P. H.; Gorina, S.; Marechal, V.; Elenbaas, B.; Moreau, J.; Levine, A. J.; Pavletich, N. P. Structure of the MDM2 oncoprotein bound to the p53 tumor suppressor transactivation domain. *Science* **1996**, *274* (5289), 948−53.
(8) Banner, D. W.; D'Arcy, A.; Janes, W.; Gentz, R.; Schoenfeld, H. J.; Broger, C.; Loetscher, H.; Lesslauer, W. Crystal structure of the soluble human 55 kd TNF receptor-human TNF beta complex: implications for TNF receptor activation. *Cell* **1993**, *73* (3), 431−45.
(9) Sattler, M.; Liang, H.; Nettesheim, D.; Meadows, R. P.; Harlan, J. E.; Eberstadt, M.; Yoon, H. S.; Shuker, S. B.; Chang, B. S.; Minn, A. J.; Thompson, C. B.; Fesik, S. W. Structure of Bcl-xL-Bak peptide complex: recognition between regulators of apoptosis. *Science* **1997**, *275* (5302), 983−6.
(10) Mosyak, L.; Zhang, Y.; Glasfeld, E.; Haney, S.; Stahl, M.; Seehra, J.; Somers, W. S. The bacterial cell-division protein ZipA and its interaction with an FtsZ fragment revealed by X-ray crystallography. *EMBO J.* **2000**, *19* (13), 3179−91.
(11) Graves, B.; Thompson, T.; Xia, M.; Janson, C.; Lukacs, C.; Deo, D.; Di Lello, P.; Fry, D.; Garvie, C.; Huang, K. S.; Gao, L.; Tovar, C.; Lovey, A.; Wanner, J.; Vassilev, L. T. Activation of the p53 pathway by small-molecule-induced MDM2 and MDMX dimerization. *Proc. Natl. Acad. Sci. U. S. A.* **2012**, *109* (29), 11788−93.
(12) Chene, P. Inhibiting the p53-MDM2 interaction: an important target for cancer therapy. *Nat. Rev. Cancer* **2003**, *3* (2), 102−9.
(13) Duncan, S. J.; Cooper, M. A.; Williams, D. H. Binding of an inhibitor of the p53/MDM2 interaction to MDM2. *Chem. Commun. (Cambridge, U. K.)* **2003**, *3*, 316−7.
(14) Dickens, M. P.; Fitzgerald, R.; Fischer, P. M. Small-molecule inhibitors of MDM2 as new anticancer therapeutics. *Semin. Cancer Biol.* **2010**, *20* (1), 10−8.
(15) Allen, J. G.; Bourbeau, M. P.; Wohlhieter, G. E.; Bartberger, M. D.; Michelsen, K.; Hungate, R.; Gadwood, R. C.; Gaston, R. D.; Evans, B.; Mann, L. W.; Matison, M. E.; Schneider, S.; Huang, X.; Yu, D.; Andrews, P. S.; Reichelt, A.; Long, A. M.; Yakowec, P.; Yang, E. Y.; Lee, T. A.; Oliner, J. D. Discovery and optimization of chromeno-triazolopyrimidines as potent inhibitors of the mouse double minute 2-tumor protein 53 protein-protein interaction. *J. Med. Chem.* **2009**, *52* (22), 7044−53.
(16) Lawrence, H. R.; Li, Z.; Yip, M. L.; Sung, S. S.; Lawrence, N. J.; McLaughlin, M. L.; McManus, G. J.; Zaworotko, M. J.; Sebti, S. M.; Chen, J.; Guida, W. C. Identification of a disruptor of the MDM2-p53 protein-protein interaction facilitated by high-throughput in silico docking. *Bioorg. Med. Chem. Lett.* **2009**, *19* (14), 3756−9.
(17) Bowman, A. L.; Nikolovska-Coleska, Z.; Zhong, H.; Wang, S.; Carlson, H. A. Small molecule inhibitors of the MDM2-p53 interaction discovered by ensemble-based receptor models. *J. Am. Chem. Soc.* **2007**, *129* (42), 12809−14.
(18) Lu, Y.; Nikolovska-Coleska, Z.; Fang, X.; Gao, W.; Shangary, S.; Qiu, S.; Qin, D.; Wang, S. Discovery of a nanomolar inhibitor of the human murine double minute 2 (MDM2)-p53 interaction through an integrated, virtual database screening strategy. *J. Med. Chem.* **2006**, *49* (13), 3759−62.
(19) Dezi, C.; Carotti, A.; Magnani, M.; Baroni, M.; Padova, A.; Cruciani, G.; Macchiarulo, A.; Pellicciari, R. Molecular interaction fields and 3D-QSAR studies of p53-MDM2 inhibitors suggest additional features of ligand-target interaction. *J. Chem. Inf. Model.* **2010**, *50* (8), 1451−65.
(20) Lu, F.; Chi, S. W.; Kim, D. H.; Han, K. H.; Kuntz, I. D.; Guy, R. K. Proteomimetic libraries-design, synthesis, and evaluation of p53-MDM2 interaction inhibitors. *J. Comb. Chem.* **2006**, *8* (3), 315−25.
(21) Herold, J. M.; Wigle, T. J.; Norris, J. L.; Lam, R.; Korboukh, V. K.; Gao, C.; Ingerman, L. A.; Kireev, D. B.; Senisterra, G.; Vedadi, M.; Tripathy, A.; Brown, P. J.; Arrowsmith, C. H.; Jin, J.; Janzen, W. P.; Frye, S. V. Small-molecule ligands of methyl-lysine binding proteins. *J. Med. Chem.* **2011**, *54* (7), 2504−11.
(22) Manepalli, S.; Geffert, L. M.; Surratt, C. K.; Madura, J. D. Discovery of novel selective serotonin reuptake inhibitors through development of a protein-based pharmacophore. *J. Chem. Inf. Model.* **2011**, *51* (9), 2417−26.
(23) Kojima, K.; Burks, J. K.; Arts, J.; Andreeff, M. The novel tryptamine derivative JNJ-26854165 induces wild-type p53- and E2F1-mediated apoptosis in acute myeloid and lymphoid leukemias. *Mol. Cancer Ther.* **2010**, *9* (9), 2545−57.
(24) Vu, B.; Wovkulich, P.; Pizzolato, G.; Lovey, A.; Ding, Q.; Jiang, N.; Liu, J.-J.; Zhao, C.; Glenn, K.; Wen, Y.; Tovar, C.; Packman, K.; Vassilev, L.; Graves, B. Discovery of RG7112: a small-molecule MDM2 inhibitor in clinical development. *ACS Med. Chem. Lett.* **2013**, *4* (5), 466−9.
(25) Yu, S.; Qin, D.; Shangary, S.; Chen, J.; Wang, G.; Ding, K.; McEachern, D.; Qiu, S.; Nikolovska-Coleska, Z.; Miller, R.; Kang, S.; Yang, D.; Wang, S. Potent and orally active small-molecule inhibitors of the MDM2-p53 interaction. *J. Med. Chem.* **2009**, *52* (24), 7970−3.
(26) Grasberger, B. L.; Lu, T.; Schubert, C.; Parks, D. J.; Carver, T. E.; Koblish, H. K.; Cummings, M. D.; LaFrance, L. V.; Milkiewicz, K. L.; Calvo, R. R.; Maguire, D.; Lattanze, J.; Franks, C. F.; Zhao, S.; Ramachandren, K.; Bylebyl, G. R.; Zhang, M.; Manthey, C. L.; Petrella, E. C.; Pantoliano, M. W.; Deckman, I. C.; Spurlino, J. C.; Maroney, A. C.; Tomczuk, B. E.; Molloy, C. J.; Bone, R. F. Discovery and cocrystal structure of benzodiazepinedione HDM2 antagonists that activate p53 in cells. *J. Med. Chem.* **2005**, *48* (4), 909−12.
(27) Bernard, D.; Zhao, Y.; Wang, S. AM-8553: A novel MDM2 inhibitor with a promising outlook for potential clinical development. *J. Med. Chem.* **2012**, *55* (11), 4934−5.
(28) Wolber, G.; Langer, T. LigandScout: 3-D pharmacophores derived from protein-bound ligands and their use as virtual screening filters. *J. Chem. Inf. Model.* **2004**, *45* (1), 160−9.
(29) Spassov, V. Z.; Flook, P. K.; Yan, L. LOOPER: a molecular mechanics-based algorithm for protein loop prediction. *Protein Eng. Des. Sel.* **2008**, *21* (2), 91−100.
(30) Spassov, V. Z.; Yan, L. A fast and accurate computational approach to protein ionization. *Protein Sci.* **2008**, *17* (11), 1955−70.
(31) Böhm, H.-J. The computer program LUDI: A new method for the de novo design of enzyme inhibitors. *J. Comput.-Aided. Mol. Des.* **1992**, *6* (1), 61−78.
(32) Anighoro, A.; Rastelli, G. Enrichment factor analyses on G-protein coupled receptors with known crystal structure. *J. Chem. Inf. Model.* **2013**, *53* (4), 739−43.
(33) Congreve, M.; Carr, R.; Murray, C.; Jhoti, H. A 'rule of three' for fragment-based lead discovery? *Drug Discovery Today* **2003**, *8* (19), 876−7.
(34) Thilagavathi, R.; Mancera, R. L. Ligand−protein cross-docking with water molecules. *J. Chem. Inf. Model.* **2010**, *50* (3), 415−21.
(35) Zhang, Q.; Lu, H. Identification of small molecules affecting p53-MDM2/MDMX interaction by fluorescence polarization. *Methods Mol. Biol.* **2013**, *962*, 95−111.
(36) Zhang, R.; Mayhood, T.; Lipari, P.; Wang, Y.; Durkin, J.; Syto, R.; Gesell, J.; McNemar, C.; Windsor, W. Fluorescence polarization assay and inhibitor design for MDM2/p53 interaction. *Anal. Biochem.* **2004**, *331* (1), 138−46.
(37) Czarna, A.; Popowicz, G. M.; Pecak, A.; Wolf, S.; Dubin, G.; Holak, T. A. High affinity interaction of the p53 peptide-analogue with human Mdm2 and Mdmx. *Cell Cycle* **2009**, *8* (8), 1176−84.
(38) Zhuang, C.; Miao, Z.; Zhu, L.; Dong, G.; Guo, Z.; Wang, S.; Zhang, Y.; Wu, Y.; Yao, J.; Sheng, C.; Zhang, W. Discovery, synthesis, and biological evaluation of orally active pyrrolidone derivatives as novel inhibitors of p53-MDM2 protein-protein interaction. *J. Med. Chem.* **2012**, *55* (22), 9630−42.
(39) Popowicz, G. M.; Czarna, A.; Wolf, S.; Wang, K.; Wang, W.; Domling, A.; Holak, T. A. Structures of low molecular weight inhibitors bound to MDMX and MDM2 reveal new approaches for p53-MDMX/MDM2 antagonist drug discovery. *Cell Cycle* **2010**, *9* (6), 1104−11.
(40) Nikolovska-Coleska, Z.; Wang, R.; Fang, X.; Pan, H.; Tomita, Y.; Li, P.; Roller, P. P.; Krajewski, K.; Saito, N. G.; Stuckey, J. A.;

Wang, S. Development and optimization of a binding assay for the XIAP BIR3 domain using fluorescence polarization. *Anal. Biochem.* **2004**, *332* (2), 261−73.
(41) Galatin, P. S.; Abraham, D. J. QSAR: hydropathic analysis of inhibitors of the p53−mdm2 interaction. *Proteins* **2001**, *45* (3), 169−75.
(42) de Vega, M. J.; Martín-Martínez, M.; González-Muñiz, R. Modulation of protein-protein interactions by stabilizing/mimicking protein secondary structure elements. *Curr. Top. Med. Chem.* **2007**, *7* (1), 33−62.
(43) Verkhivker, G. M. Simulating molecular mechanisms of the MDM2-mediated regulatory interactions: a conformational selection model of the MDM2 lid dynamics. *PLoS One* **2012**, *7* (7), e40897.
(44) Vassilev, L. T.; Vu, B. T.; Graves, B.; Carvajal, D.; Podlaski, F.; Filipovic, Z.; Kong, N.; Kammlott, U.; Lukacs, C.; Klein, C.; Fotouhi, N.; Liu, E. A. In vivo activation of the p53 pathway by small-molecule antagonists of MDM2. *Science* **2004**, *303* (5659), 844−8.
(45) Grasberger, B. L.; Lu, T.; Schubert, C.; Parks, D. J.; Carver, T. E.; Koblish, H. K.; Cummings, M. D.; LaFrance, L. V.; Milkiewicz, K. L.; Calvo, R. R.; Maguire, D.; Lattanze, J.; Franks, C. F.; Zhao, S.; Ramachandren, K.; Bylebyl, G. R.; Zhang, M.; Manthey, C. L.; Petrella, E. C.; Pantoliano, M. W.; Deckman, I. C.; Spurlino, J. C.; Maroney, A. C.; Tomczuk, B. E.; Molloy, C. J.; Bone, R. F. Discovery and cocrystal structure of benzodiazepinedione HDM2 antagonists that activate p53 in cells. *J. Med. Chem.* **2005**, *48* (4), 909−12.
(46) Hu, B.; Lill, M. A. Protein pharmacophore selection using hydration-site analysis. *J. Chem. Inf. Model.* **2012**, *52* (4), 1046−60.
(47) Lauria, A.; Tutone, M.; Ippolito, M.; Pantano, L.; Almerico, A. M. Molecular modeling approaches in the discovery of new drugs for anti-cancer therapy: the investigation of p53-MDM2 interaction and its inhibition by small molecules. *Curr. Med. Chem.* **2010**, *17* (28), 3142−54.
(48) Almerico, A. M.; Tutone, M.; Pantano, L.; Lauria, A. Molecular dynamics studies on Mdm2 complexes: an analysis of the inhibitor influence. *Biochem. Biophys. Res. Commun.* **2012**, *424* (2), 341−7.
(49) Lipinski, C. A.; Lombardo, F.; Dominy, B. W.; Feeney, P. J. Experimental and computational approaches to estimate solubility and permeability in drug discovery and development settings. *Adv. Drug Delivery Rev.* **2001**, *46* (1−3), 3−26.
(50) Cheng, F.; Li, W.; Zhou, Y.; Shen, J.; Wu, Z.; Liu, G.; Lee, P. W.; Tang, Y. admetSAR: a comprehensive source and free tool for assessment of chemical ADMET properties. *J. Chem. Inf. Model.* **2012**, *52* (11), 3099−105.
(51) Cao, D.; Wang, J.; Zhou, R.; Li, Y.; Yu, H.; Hou, T. ADMET evaluation in drug discovery. 11. PharmacoKinetics Knowledge Base (PKKB): a comprehensive database of pharmacokinetic and toxic properties for drugs. *J. Chem. Inf. Model.* **2012**, *52* (5), 1132−7.
(52) Showalter, S. A.; Bruschweiler-Li, L.; Johnson, E.; Zhang, F.; Bruschweiler, R. Quantitative lid dynamics of MDM2 reveals differential ligand binding modes of the p53-binding cleft. *J. Am. Chem. Soc.* **2008**, *130* (20), 6472−8.